AIAA AVIATION Forum
August 2-6, 2021, VIRTUAL EVENT
AIAA AVIATION 2021 FORUM

10.2514/6.2021-2591

Lift Enhancement of Supersonic Thin Airfoil at Low Speed by Co-Flow Jet Active Flow Control

Zhijin Lei * Gecheng Zha †
Dept. of Mechanical and Aerospace Engineering
University of Miami, Coral Gables, Florida 33124
E-mail: gzha@miami.edu

Abstract

This paper numerically studies a lift enhancement approach for a supersonic thin airfoil with t/c of 3.2% using Co-Flow Jet (CFJ) active flow control at Mach number of 0.1. The Reynolds averaged Navier-Stokes equations with Spalart-Allmaras turbulence model are solved with high order accuracy numerical schemes. The CFJ is first applied to the flapless airfoil. It is able to achieve a high lift coefficient of 2.12 at an angle of incidence of 18deg, 141.9% higher than the baseline airfoil, but at a very large CFJ power cost with the CFJ power coefficient of 3.06. By using a flap for the baseline and CFJ airfoil at zero angle of incidence, the lift coefficient can be increased much more efficiently than using a flapless airfoil. Two methods applying CFJ on the flapped airfoil are investigated: 1) using CFJ on the front main part of the flapped airfoil; 2) using CFJ on both the front part and on the flap. For the same momentum coefficient C_μ of 0.08, the methods 2 achieves a high lift coefficient of 1.91, 42.5% higher than that of the method 1, with a CFJ power coefficient of 0.085, 7.6% lower than that of the method 1. The C_L/C_D and $(C_L/C_D)_c$ for the CFJ method 2 is 20 and 10.6, respectively. Compared with the baseline flapped airfoil with no flow control, the lift increase is 103% with a $(C_L/C_D)_c$ increase of 5.5%, which results in a productivity efficiency increase of 114.2%. Such a good aerodynamic performance is attributed to splitting the CFJ to two series CFJs in streamwise direction with C_μ of 0.024 used in the front and 0.056 used on the flap. The front CFJ mitigates the separation bubble on the front part of the thin airfoil and energizes the flow, the rear CFJ attaches the flow efficiently in adverse pressure gradients. Even though the total C_μ of 0.08 is the same for the CFJ method 1 and 2, each of the CFJ in the method 2 has a lower total pressure loss and thus requires lower total pressure ratio from the CFJ actuators, which reduces the total CFJ power required. Using two CFJs in series in the streamwise direction provides a high effectiveness and high efficiency lift enhancement method for supersonic thin airfoil. More study needs to be done to understand the interaction relationship between the two CFJs.

Nomenclature

CFJ	Co-flow Jet
SST	Supersonic (Civil) Transports
SST	Suction Surface Translation
AoA	Angle of Attack
LE	Leading Edge
TE	Trailing Edge
Ma	Mach Number

* Graduate Student
† Professor, ASME Fellow, AIAA associate Fellow

U	Flow Velocity
P	Pumping Power
C_L	Lift Coefficient $L/(q_\infty S)$
C_D	Drag Coefficient $D/(q_\infty S)$
C_μ	Jet Momentum Coefficient $\dot{m}_j U_j/(q_\infty S)$
$(C_L/C_D)_c$	CFJ Corrected Lift-Drag Ratio $L/(q_\infty S V_\infty)$
S_{wing}	Wing Area
$S_{Takeoff}$	Takeoff Distance
$\dot{m}$	Mass Flow
c	Chord Length
q	Dynamic Pressure $0.5\,\rho U^2$
p_t	Mass-averaged Static Pressure
α	Angle of Incidence
β	Flap deflection Angle
γ	Specific Heat Ratio
η	Pump Efficiency
ρ	Air Density
∞	Free Stream Conditions
$_j$	Jet Conditions

1 Introduction

Supersonic Civil Transports (SST) is an important sector in aviation industry. High efficiency and low sonic boom are crucial for the SST's economic viability. The higher the cruise speed, the more difficult to meet the stringent requirements of low speed, which determines the community noise and runway length. One challenge for supersonic aircraft at low speed is to achieve a high lift coefficient, which is difficult to obtain when the wing is highly swept and formed with thin airfoil and high aspect ratio.

As shown in Table 1, Concorde needs a runway of about 12,000 ft to take off, which almost exceeds the longest runway of the New York JFK Airport. NASA's SST N+2 Program expects that 30-passenger supersonic business jets and 100-passenger commercial jets limit their takeoff runway requirements to be less than 9,000 fts[1].

Table 1: C_{Lmax}, S_{wing}, $S_{Takeoff}$ and Takeoff Velocity of Existing SSTs, compared with B767-200ER.

Aircraft	Weight, lb	C_{Lmax}	S_{wing}, ft^2	$S_{Takeoff}$, ft	Takeoff Velocity, mph
Tu-144LL[2, 3]	455,950	0.612	5,450	9,613	220
Concorde[4]	400,000	0.77	3,856	11,800	250
B767-200ER[5]	395,000	$\simeq 2$	3,050	8,150	140-190(B767-300)

Table 1 shows the maximum takeoff lift coefficient, wing area and required takeoff runway length of Concorde, Tu-144LL and B767-200ER(as comparison). It can be seen that, if the maximum lift coefficient of the two SST during takeoff can be increased to the level of transonic transports, the run way length can be reduced to below 9,000 ft.

Mavris *et al*[6] employ Circulation Control (CC) flow control to enhance HSCT low speed lift coefficient based on the work of Englar[7]. For some configurations, the CC can reduce the takeoff field length by 31%, the liftoff

speed by 11%, and the obstacle height speed by 10%. However, CC needs to use engine bleed, which may be difficult to obtain at takeoff when the engines need maximum mass flow for maximum thrust, and at landing when the engines are mostly idle.

The purpose of this paper is to enhance the lift coefficient of 2D thin supersonic airfoil at low speeds by using coflow jet active flow control with minimized energy expenditure. The study is important to lay a foundation for 3D supersonic swept wing lift enhancement at takeoff and landing[8].

1.1 Co-Flow Jet (CFJ) Active Flow Control

The CFJ developed by Zha *et al*[9, 10, 11, 12, 13, 14, 15, 16, 17, 18, 19, 20] is demonstrated to achieve large lift augmentation, stall margin increase, drag reduction and moderate nose-down moment for stationary and pitching airfoils.

In a CFJ airfoil, an injection slot near the leading edge (LE) and a suction slot near the trailing edge (TE) on the airfoil suction surface are created. As shown in Fig. 1, a small amount of mass flow is drawn into the suction duct, pressurized and energized by the micro compressor, and then injected near the LE tangentially to the main flow via an injection duct. The whole process does not add any mass flow to the system and hence is a zero-net-mass-flux(ZNMF) flow control.

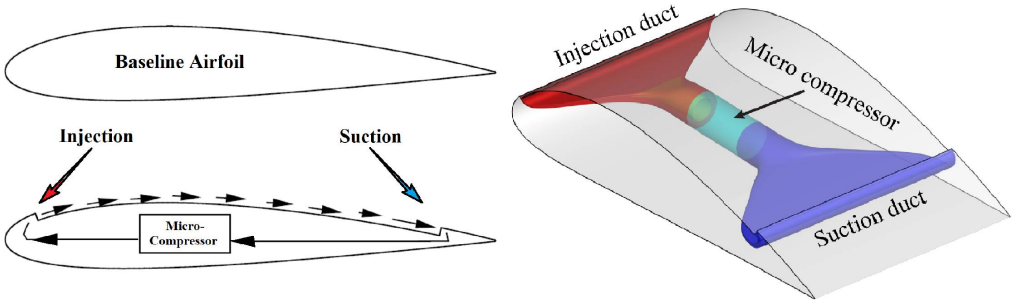

Figure 1: Schematic plot of a typical CFJ airfoil.

The research so far on CFJ are focused on thick airfoils and wings. This study is the first effort to apply CFJ to 2D thin supersonic airfoil at low speeds with or without flaps to enhance the lift coefficient with minimized CFJ power consumption.

1.1.1 CFJ Parameters

The following are some important parameters used for CFJ active flow control. The jet momentum coefficient C_μ is a parameter used to quantify the jet intensity and is defined as:

$$C_\mu = \frac{\dot{m}U_j}{\frac{1}{2}\rho_\infty {U_\infty}^2 S} \tag{1}$$

where $\dot{m}$ is the injection mass flow, V_j is the mass-averaged injection velocity, ρ_∞ and V_∞ denote the free stream density and velocity, and S is the planform area.

The power consumption is determined by the jet mass flow and total enthalpy change as the following:

$$P = \dot{m}(H_{t1} - H_{t2}) \tag{2}$$

where H_{t1} and H_{t2} are the mass-averaged total enthalpy in the injection cavity and suction cavity respectively, P is the Power required by the pump and $\dot{m}$ the jet mass flow rate.

The total power can be expressed with the pump efficiency η and total pressure ratio of the pump $\Gamma = \frac{P_{t1}}{P_{t2}}$ as:

$$P = \frac{\dot{m}C_pT_{t2}}{\eta}(\Gamma^{\frac{\gamma-1}{\gamma}} - 1) \tag{3}$$

where γ is the specific heat ratio equal to 1.4 for air. Eq. 3 indicates that the CFJ power is determined exponentially by the total pressure ratio and linearly by the mass flow rate. This provides a guideline to minimize the energy expenditure by using larger injection slot size to have lower total pressure loss and higher mass flow[21, 22, 23, 24, 25, 26].

The power coefficient is expressed as:

$$P_c = \frac{P}{\frac{1}{2}\rho_\infty V_\infty^3 S} \tag{4}$$

For a CFJ wing, a corrected aerodynamic efficiency that includes the CFJ power coefficient is defined as:

$$(\frac{C_L}{C_D})_c = \frac{C_L}{C_D + P_c} \tag{5}$$

Eq. 5 is mainly for the purpose to compare the aerodynamic efficiency with conventional aircraft with no active flow control that has $P_c = 0$. A more comprehensive parameter termed productivity efficiency measuring the aircraft transportation productivity represented by $R \times W$ (Range $\times$ Gross weight) is defined as[22]:

$$(\frac{C_L^2}{C_D})_c = \frac{C_L^2}{C_D + P_c} \tag{6}$$

2 The Airfoils

The baseline airfoil, shown in Fig. 2, is a thin symmetric airfoil we created with a maximum thickness of 3.2%chord to represent a supersonic airfoil, named OD3P. For CFJ airfoil, we usually have the suction surface (upper surface) slightly translated downward to accommodate the tangential injection jet. It is named suction surface translation (SST).

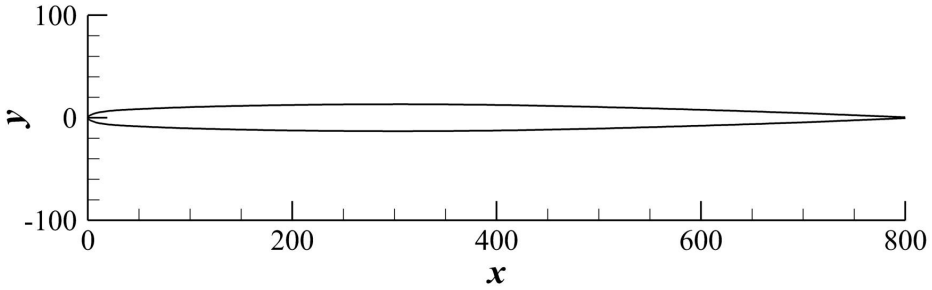

Figure 2: Baseline geometry.

Fig. 3 shows the 2D thin airfoils modified from OD3P studied in this paper. They include two groups: flapless airfoil shown on the top row of Fig. 3 and the flapped airfoils shown on the lower part. Each group has a baseline airfoil with no CFJ for comparison. The flapless CFJ airfoil uses the Geometry D, CFJ-OD3P-0-0.5-75-8-0 shown on the right upper corner of Fig. 3, which has injection slot located at 0.5%C with a size of 0.3%C and suction slot located at 75%C with a size of 1%C. The flapped baseline airfoil is modified from the flapless baseline airfoil by adding a hinge at 80%C location. The CFJ flapped airfoils are modified from the Geometry D by adding a hinge at 80%C location and have two different types: CFJ-1 and CFJ-2. The CFJ-1 airfoil only has the CFJ applied on the front main part of the airfoil and the flap has no flow control. The CFJ-2 configuration has CFJ applied on both the main part and the flap. A flow angle of incidence α is used to define the angle between the freestream direction and the chord of the front main part of a flapped airfoil as illustrated in Fig. 3. For flapless airfoil, the angle of incidence is the same as the angle of attack.

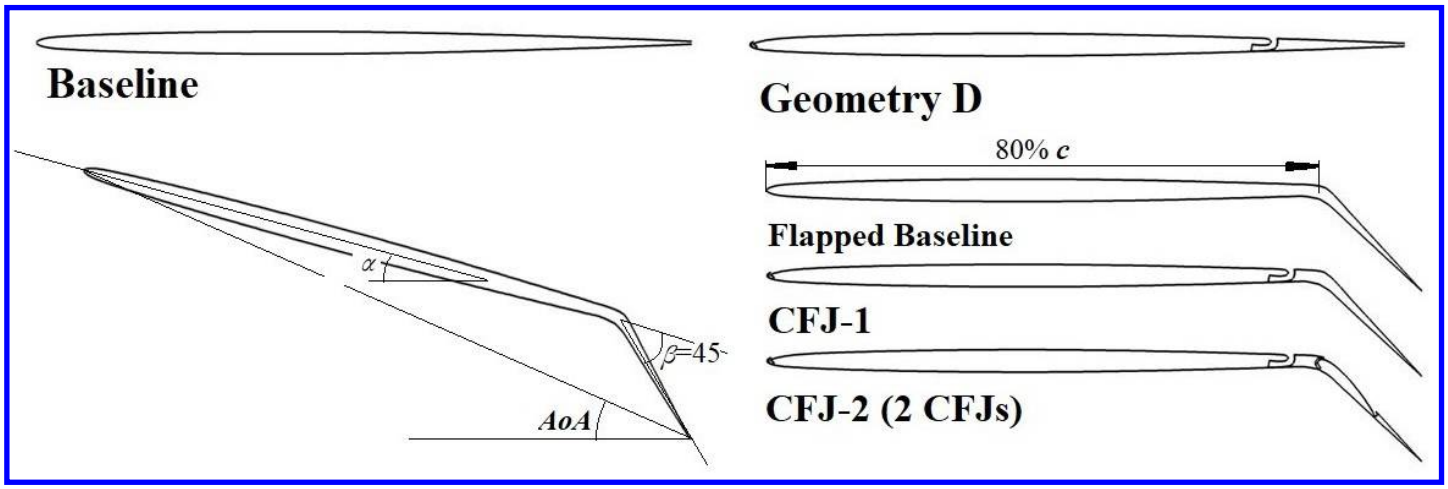

Figure 3: Configurations of the flapless and flapped airfoils without and with CFJ.

3 Numerical Approaches

The in-house CFD code FASIP (Flow-Acoustics-Structure Interaction Package) is used to conduct all the numerical simulations. The 2-D Reynolds-Averaged Navier-Stokes (RANS) equation is solved with one-equation Spalart-Allmaras turbulence model. A 5th order WENO scheme for the inviscid flux and a 2nd order central differencing for the viscous terms are employed to discretize the Navier-Stokes equations. The low diffusion E-CUSP scheme used as the approximate Riemann solver suggested by Zha *et al*[27] based on the Zha-Bilgen flux

vector splitting scheme [28] is utilized with the WENO scheme to evaluate the inviscid fluxes. Implicit time marching method using Gauss-Seidel line relaxation is adopted to achieve a fast convergence rate [29]. Parallel computing is implemented to save wall-clock simulation time. The RANS solver is validated for CFJ airfoil simulation[30, 13, 14, 15, 16, 17, 18, 19, 20, 21, 22, 23, 24, 25, 26].

The wall treatment suggested in [31] to achieve the 3rd order accuracy is employed. Total pressure, total temperature and flow angle are specified as the inlet boundary conditions for the upstream side of the far-field boundary and inside the injection cavity. Constant static pressure is used downstream at the far-field boundary and in the suction cavity. To achieve zero-net mass-flux with the CFJ flow control, the injection mass flow must be equal to the mass flow entering the suction slot. Additionally, the jet strength must be controlled in order to reach the prescribed C_μ. This is achieved by iterating the jet total pressure until the C_μ value is within 1% of the prescribed value. At the suction, the suction mass flow is matched to the injection mass flow by iterating the static pressure at the suction cavity. The process is iterated throughout the simulation until the specified momentum coefficient is achieved and the injection and suction mass flow match.

3.1 Mesh

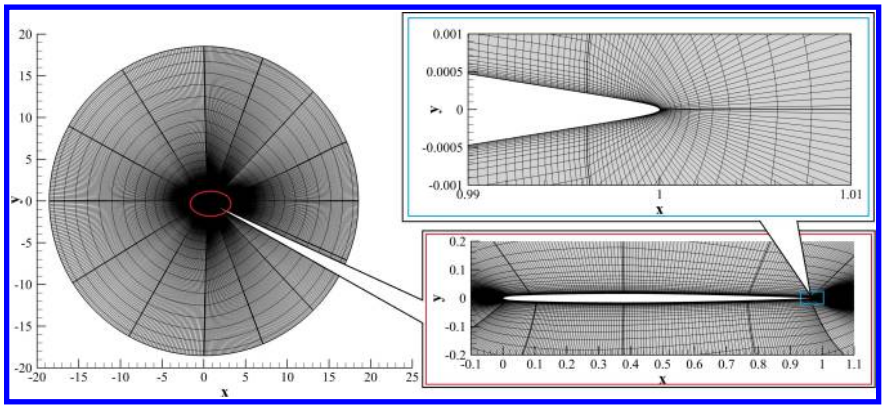

Figure 4: A baseline mesh.

The computational mesh is constructed using an O-mesh topology in order to achieve high quality around the airfoil. The O-mesh is split into 14 blocks for parallel computing. To resolve the turbulent boundary layer, the thickness of the first layer around the surface has $y_+ = 1$. The baseline mesh has 151 points in the i direction around the airfoil and 61 points in the j radial direction.

Three refined meshes are used for mesh refinement study with the size of 300 $\times$ 60, 300 $\times$ 120 and 600 $\times$ 60. The coefficient of lift and drag of the results from different meshes are shown in Fig. 5. It shows that, the 300 $\times$ 60 mesh is sufficient to have a mesh independent solution and is used for all the studies in this paper.

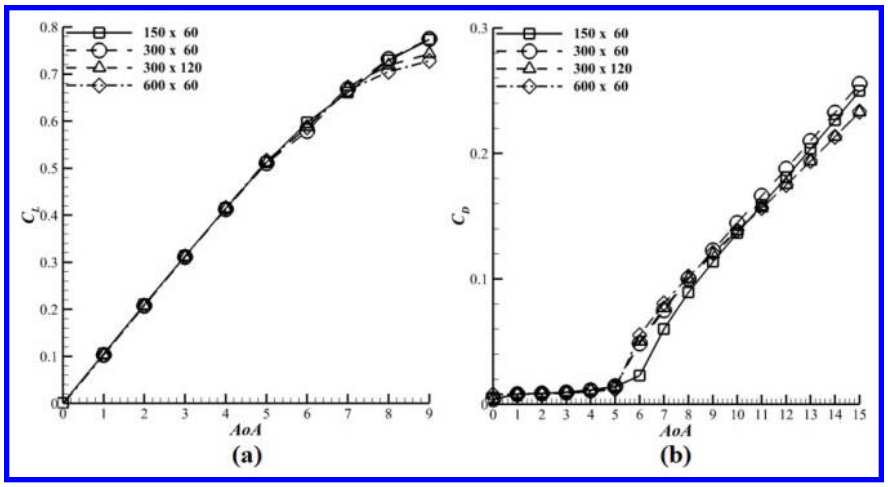

Figure 5: Baseline C_L, C_D Mesh-independence validation. Ma=0.1, α=0°, Re=2.85×10^6.

4 Results and Discussion

The free-stream condition used are Ma_∞=0.1 and Re = 2.85 × 10^6. Fig. 6 (a)-(c) shows the flapless baseline and CFJ airfoil Mach contours with streamlines at angles of incidence of 7°, 12°, and 18° with the corresponding C_μ that achieves mostly attached flows. Table 3 lists the quantitative results. The baseline airfoil at α of 7° has a thin flow separation starting from the leading edge and extend to the trailing edge. When α is increased to 12° and 18°, the separation is massive. The CFJ airfoil using C_μ of 0.08, 0.3, and 0.5 mostly removes the flow separation from the macro scale, but downstream of the leading edge of the CFJ airfoil, there is a small flow separation, which has the effect of rounding and thickening the airfoil.

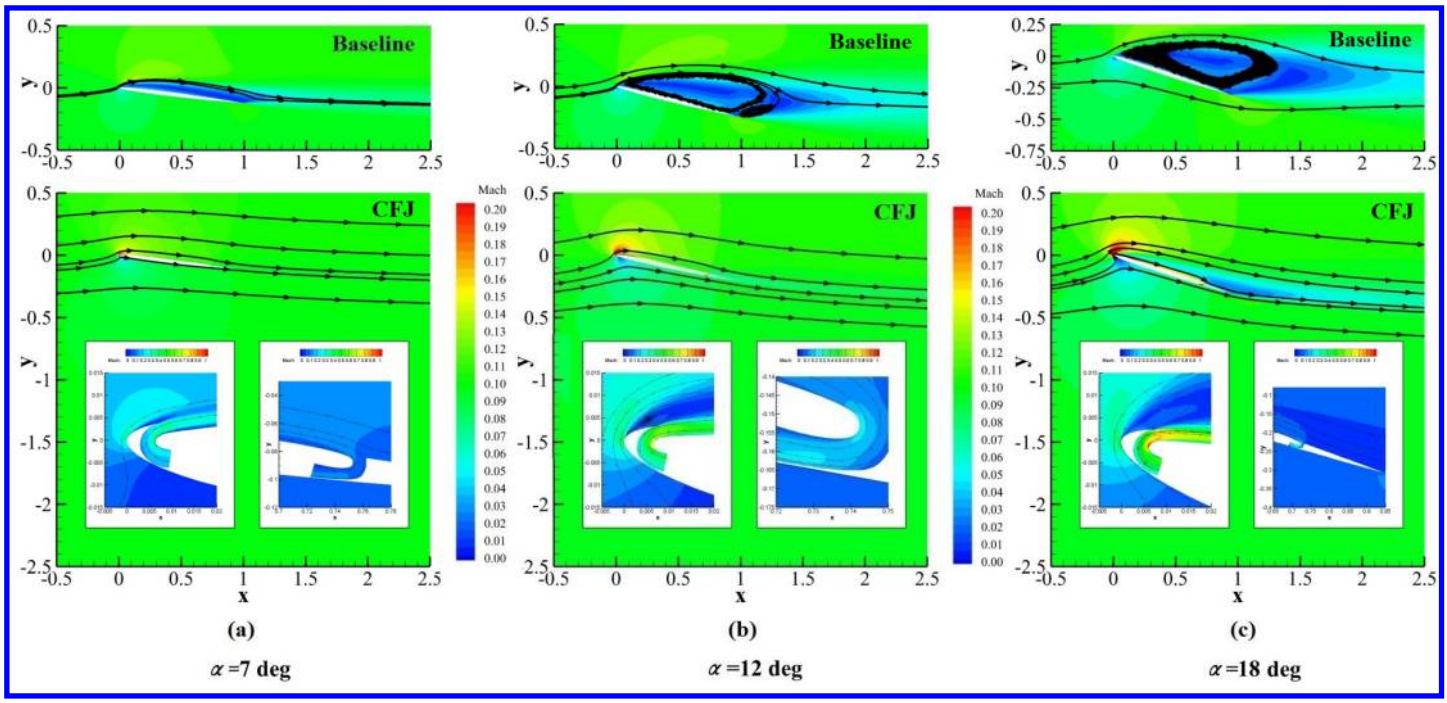

Figure 6: Mach contour of the baseline airfoil and CFJ geometry D at varied αs and corresponding C_μ.

Table 3 indicates that the CFJ thin airfoil is able to achieve a large lift coefficient increase from 21.6% to 141.9% when the incidence is varied from 7° to 18°. The airfoil generates a thrust of C_D from -0.011 to -0.027. At low α of 7°, not just the C_L is improved by 21.6%, the corrected aerodynamic efficiency also exceeds that of the baseline by 14.55%, which results in a 39% productivity efficiency improvement. At high α, the large lift enhancement comes with a high cost of energy with the CFJ power coefficient up to 3.05.

Table 2: Comparison of baseline and CFJ thin airfoil at different α and C_μ

Case	α	C_μ	C_L	δC_L	C_D	P_c	C_L/C_D	$(C_L/C_D)_c$	$\delta(C_L/C_D)_c$
Baseline	7°	0	0.666	-	0.081	0	8.25	8.25	-
CFJ	7°	0.08	0.810	21.6%	-0.011	0.097	-73.64	9.45	14.55%
Baseline	12°	0	0.778	-	0.175	0	4.44	4.44	-
CFJ	12°	0.3	1.458	87.4%	-0.057	0.861	-25.58	1.81	-59.3%
Baseline	18°	0	0.878	-	0.298	0	2.95	2.95	-
CFJ	18°	0.5	2.124	141.9%	-0.027	3.055	-78.67	0.702	-66.0%

To seek an alternative way of enhancing lift coefficient of thin airfoil with high efficiency, the second group of the airfoils with flaps described in Fig. 3 are studied. Fig. 7 shows the pressure and Mach contours with streamlines of the flapped-baseline(a), CFJ-1(b) and CFJ-2(c) airfoils at α=0° and flap deflection angle of 45°. The same C_μ of 0.08 is used for the two CFJ cases. Table 3 gives the quantitative comparison.

Fig. 7 (a) indicates that the flapped-baseline airfoil flow has a separation bubble starting from the leading edge of the front part, reattaches near the end, and is massively separated in the flap region due to the large flap deflection. It has a C_L of 0.945 and C_L/C_D of 10.05, significantly better than the flapless baseline airfoil at α=7° in Table 2. The CFJ-1 with C_μ of 0.08 is able to remove the flow separation in the front part completely, but has a small flow separation on the flap. The C_L is 1.347, 42.5% higher than the baseline, and the $(C_L/C_D)_c$ is about the same as the baseline. This is a significant improvement over the flapped baseline airfoil.

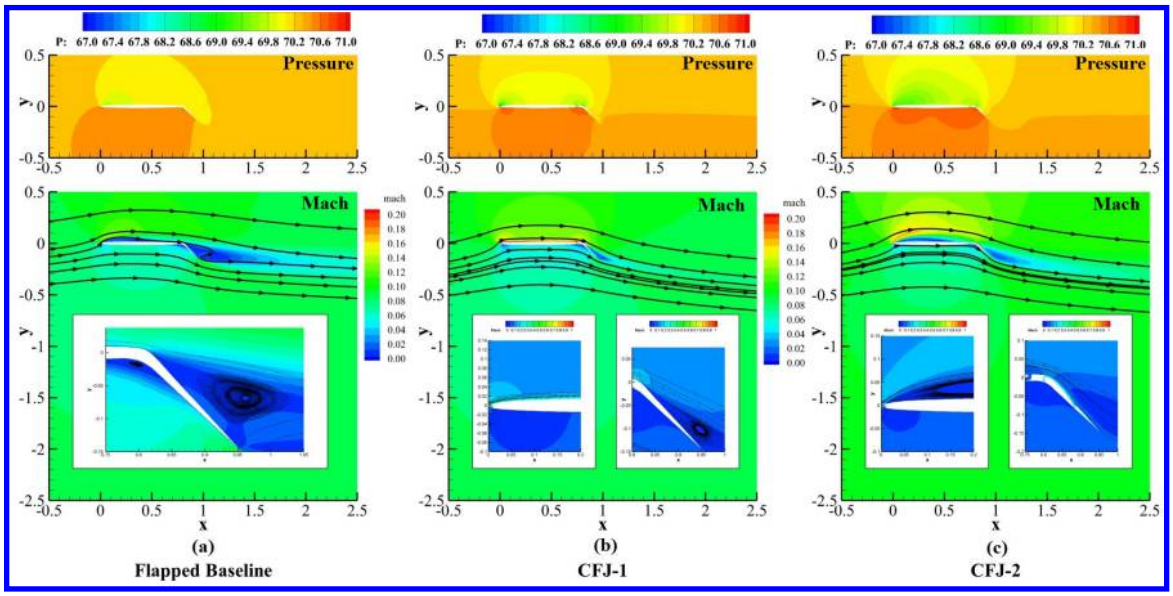

Figure 7: Pressure and Mach contour of flow fields around flapped airfoils at α=0°, C_μ=0.08.

The most encouraging result is from the CFJ-2 flapped airfoil, which has the CFJ applied on both the front

main part and on the flap. The same total C_μ of 0.08 as for the CFJ-1 is used, but is split to 0.024 for the front part and 0.056 for the flap. The front CFJ with $C_\mu u$ of 0.024 is not able to completely remove the front separation bubble, but mitigates the separation and energizes the flow, which makes the flow attached on the flap. The mild separation on the front part of the airfoil also creates a thickening effect of the airfoil that increases lift. The attached flow on the flap turns the flow locally by about 45° following the flap and significantly increases the circulation and the lift coefficient. The comparison of the pressure contours of the three cases in Fig. 7 clearly shows that the CFJ-2 has significantly higher pressure on the pressure surface and lower pressure on the suction surface than those of CFJ-1 and the flapped baseline airfoil.

Quantitatively, the CFJ-2 case achieves a C_L of 1.919, 42.5% higher than that of the CFJ-1, 103% higher than that of the flapped baseline with a 6% higher $(C_L/C_D)_c$. The excellent aerodynamic efficiency of a thin airfoil at such a high C_L is attributed to the two split CFJs that each has a lower C_μ and thus a lower total pressure ratio. As indicated by Eq. (3), the CFJ power coefficient is determined exponentially by the total pressure ratio and linearly by the mass flow rate[21, 22, 23, 24, 25, 26]. Thus even though the total C_μ is the same as that of the CFJ-1, the P_c of each individual CFJ is substantially lower, so is the total P_c as the sum. The benefit applying the CFJ on the flap is because that CFJ is most effective and efficient to be used in adverse pressure gradients as indicated by Xu et al[26].

Table 3: Lift, drag and power performance of various geometries, α=0°, C_μ=0.08.

Geometry	C_L	δC_L	C_D	P_c	C_L/C_D	$(C_L/C_D)_c$	$\delta(C_L/C_D)_c$
Baseline	0.945	0	0.094	0	10.05	10.05	0
CFJ-1	1.347	42.5%	0.043	0.092	31.33	9.98	-0.7%
CFJ-2	1.919	103.1%	0.096	0.085	19.99	10.60	5.5%

Multiple CFJ actuators are used in parallel with varying strength along 3D transonic wing span to optimize the wing efficiency by Boling and Zha[32]. The CFJ-2 case in this study is the first time using two CFJs in a series manner in the streamwise direction to enhance 2D thin airfoil lift coefficient and reduce the energy consumption. The result is encouraging, but is not optimized. More study needs to be done to understand the relationship between the two CFJs in series. This may open a new direction to optimize the CFJ effectiveness and efficiency, in particular for thin airfoils. For 3D highly swept Delta wings formed by thin airfoil, Lei and Zha [8] demonstrate that applying CFJ only on the flap is the most effective and efficient.

5 Conclusions

This paper numerically studies a lift enhancement approach for a supersonic thin airfoil with t/c of 3.2% using Co-Flow Jet (CFJ) active flow control at Mach number of 0.1. The CFJ is first applied to the flapless airfoil. It is able to achieve a high lift coefficient of 2.12 at an angle of incidence of 18deg, 141.9% higher than the baseline airfoil, but at a very large CFJ power cost with the CFJ power coefficient of 3.06. By using a flap for the baseline and CFJ airfoil at zero angle of incidence, the lift coefficient can be increased much more efficiently than using a flapless airfoil. Two methods applying CFJ on the flapped airfoil are investigated: 1) using CFJ on the front main part of the flapped airfoil; 2) using CFJ on both the front part and on the flap. For the same momentum coefficient C_μ of 0.08, the methods 2 achieves a high lift coefficient of 1.91, 42.5% higher than that of the method 1, with a CFJ power coefficient of 0.085, 7.6% lower than that of the method 1. The C_L/C_D and $(C_L/C_D)_c$ for the CFJ method 2 is 20 and 10.6, respectively. Compared with the baseline flapped airfoil with no flow control, the lift increase is 103% with a $(C_L/C_D)_c$ increase of 5.5%, which results in a productivity efficiency increase of

114.2%. Such a good aerodynamic performance is attributed to splitting the CFJ to two series CFJs in streamwise direction with C_μ of 0.024 used in the front and 0.056 used on the flap. The front CFJ mitigates the separation bubble on the front part of the thin airfoil and energizes the flow, the rear CFJ attaches the flow efficiently in adverse pressure gradients. Even though the total C_μ of 0.08 is the same for the CFJ method 1 and 2, each of the CFJ in the method 2 has a lower total pressure loss and thus requires lower total pressure ratio from the CFJ actuators, which reduces the total CFJ power required. Using two CFJs in series in the streamwise direction provides a high effectiveness and high efficiency lift enhancement method for supersonic thin airfoil. More study needs to be done to understand the interaction relationship between the two CFJs.

6 Acknowledgment

The simulations are conducted on Pegasus super-computing system at the Center for Computational Sciences (CCS) at the University of Miami.

Disclosure: The University of Miami and Dr. Gecheng Zha may receive royalties for future commercialization of the intellectual property used in this study. The University of Miami is also equity owner in CoFlow Jet, LLC, licensee of the intellectual property used in this study.

References

[1] H. Welge, C. Nelson, and J. Bonet, "Supersonic vehicle systems for the 2020 to 2035 timeframe," in *28th AIAA Applied Aerodynamics Conference*, p. 4930, 2010.

[2] R. E. Curry and L. R. Owens, "Ground-effect characteristics of the tu-144 supersonic transport airplane," 2003.

[3] R. A. Rivers, E. B. Jackson, C. G. Fullerton, T. H. Cox, and N. H. Princen, "A qualitative piloted evaluation of the tupolev tu-144 supersonic transport," 2000.

[4] E. Gordon, "Technical specs, http://www.concordesst.com/concordeb.html," 2001.

[5] D. A. Garvin, "Boeing 767: From concept to production (a)," 1988.

[6] D. Mavris and M. Kirby, "Takeoff / landing assessment of an hsct with pneumatic lift augmentation," in *37th Aerospace Sciences Meeting and Exhibit*, p. 534, 1998.

[7] R. L. L. Englar, "Circulation control for high lift and drag generation on stol aircraft," *Journal of Aircraft*, vol. 12, no. 5, pp. 457–463, 1975.

[8] Z.-J. Lei and G.-C. Zha, "Lift enhancement for highly swept 3d delta wing at low speed using coflow jet flow control." AIAA-2021-2559, AIAA Aviation 2021, Virtual Events, Aug. 2-6, 2021.

[9] G.-C. Zha and D. C. Paxton, "A Novel Flow Control Method for Airfoil Performance Enhancement Using Co-Flow Jet." *Applications of Circulation Control Technologies*, Chapter 10, p. 293-314, Vol. 214, Progress in Astronautics and Aeronautics, AIAA Book Series, Editors: Joslin, R. D. and Jones, G.S., 2006.

[10] G.-C. Zha, W. Gao, and C. Paxton, "Jet Effects on Co-Flow Jet Airfoil Performance," *AIAA Journal, No. 6,*, vol. 45, pp. 1222–1231, 2007.

[11] G.-C. Zha, C. Paxton, A. Conley, A. Wells, and B. Carroll, "Effect of Injection Slot Size on High Performance Co-Flow Jet Airfoil," *AIAA Journal of Aircraft*, vol. 43, 2006.

[12] G.-C. Zha, B. Carroll, C. Paxton, A. Conley, and A. Wells, "High Performance Airfoil with Co-Flow Jet Flow Control," *AIAA Journal*, vol. 45, 2007.

[13] Wang, B.-Y. and Haddoukessouni, B. and Levy, J. and Zha, G.-C., "Numerical Investigations of Injection Slot Size Effect on the Performance of Co-Flow Jet Airfoil," *Journal of Aircraft*, vol. Vol. 45, No. 6,, pp. pp.2084–2091, 2008.

[14] B. P. E. Dano, D. Kirk, and G.-C. Zha, "Experimental Investigation of Jet Mixing Mechanism of Co- Flow Jet Airfoil." AIAA-2010-4421, 5th AIAA Flow Control Conference, Chicago, IL, 28 Jun - 1 Jul 2010.

[15] B. P. E. Dano, G.-C. Zha, and M. Castillo, "Experimental Study of Co-Flow Jet Airfoil Performance Enhancement Using Micro Discreet Jets." AIAA Paper 2011-0941, 49th AIAA Aerospace Sciences Meeting, Orlando, FL, 4-7 January 2011.

[16] A. Lefebvre, B. Dano, W. Bartow, M. Fronzo, and G. Zha, "Performance and energy expenditure of coflow jet airfoil with variation of mach number," *Journal of Aircraft*, vol. 53, no. 6, pp. 1757–1767, 2016.

[17] A. Lefebvre, G-C. Zha, "Numerical Simulation of Pitching Airfoil Performance Enhancement Using Co-Flow Jet Flow Control," *AIAA paper 2013-2517*, June 2013.

[18] A. Lefebvre, G-C. Zha, "Cow-Flow Jet Airfoil Trade Study Part I : Energy Consumption and Aerodynamic Performance," *32nd AIAA Applied Aerodynamics Conference, AIAA AVIATION Forum, AIAA 2014-2682*, June 2014.

[19] A. Lefebvre, G-C. Zha, "Cow-Flow Jet Airfoil Trade Study Part II : Moment and Drag," *32nd AIAA Applied Aerodynamics Conference, AIAA AVIATION Forum, AIAA 2014-2683*, June 2014.

[20] Lefebvre, A. and Zha, G.-C., "Trade Study of 3D Co-Flow Jet Wing for Cruise Performance." AIAA Paper 2016-0570, AIAA SCITECH2016, AIAA Aerospace Science Meeting, San Diego, CA, 4-8 January 2016.

[21] Lefebvre, A. and Dano, B. and Bartow, W. and Di Franzo, M. and Zha, G.-C., "Performance Enhancement and Energy Expenditure of Co-Flow Jet Airfoil with Variation of Mach Number." AIAA Paper 2013-0490, AIAA Journal of Aircraft, DOI: 10.2514/1.C033113, 2016.

[22] Yunchao Yang and Gecheng Zha, "Super-Lift Coefficient of Active Flow Control Airfoil: What is the Limit?." AIAA Paper 2017-1693, AIAA SCITECH2017, 55th AIAA Aerospace Science Meeting, Grapevine, January 9-13 2017.

[23] Y. Wang and G.-C. Zha, "Study of 3D Co-flow Jet Wing Induced Drag and Power Consumption at Cruise Conditions." AIAA Paper 2019-0034, AIAA SciTech 2019, San Diego, CA, January 7-11, 2019.

[24] Y. Wang, Y.-C. Yang, and G.-C. Zha, "Study of Super-Lift Coefficient of Co-Flow Jet Airfoil and Its Power Consumption." AIAA Paper 2019-3652, AIAA Aviation 2019, AIAA Applied Aerodynamics Conference, Dallas, Texas, 17-21 June 2019.

[25] Y. Wang and G.-C. Zha, "Study of Mach Number Effect for 2D Co-Flow Jet Airfoil at Cruise Conditions." AIAA Paper 2019-3169, AIAA Aviation 2019, AIAA Applied Aerodynamics Conference, Dallas, Texas, 17-21 June 2019.

[26] K.-W. Xu, Y. Ren, and G.-C. Zha, "Flow separation control by coflow wall jet." AIAA Paper 2021-2946, AIAA Aviation 2021, Virtual Events, Submitted to AIAA Journal, 2-6 Aug. 2021.

[27] Zha, G.C., Shen, Y.Q. and Wang, B.Y., "An improved low diffusion E-CUSP upwind scheme ," *Journal of Computer and Fluids*, vol. 48, pp. 214–220, Sep. 2011.

[28] G.-C. Zha and E. Bilgen, "Numerical Solutions of Euler Equations by Using a New Flux Vector Splitting Scheme ," *International Journal for Numerical Methods in Fluids*, vol. 17, pp. 115–144, 1993.

[29] G.-C. Zha and E. Bilgen, "Numerical Study of Three-Dimensional Transonic Flows Using Unfactored Upwind-Relaxation Sweeping Algorithm," *Journal of Computational Physics*, vol. 125, pp. 425–433, 1996.

[30] B.-Y. Wang and G.-C. Zha, "A General Sub-Domain Boundary Mapping Procedure For Structured Grid CFD Parallel Computation," *AIAA Journal of Aerospace Computing, Information, and Communication*, vol. 5, No.11, pp. 2084–2091, 2008.

[31] Y.-Q. Shen, G.-C. Zha, and B.-Y. Wang, "Improvement of Stability and Accuracy of Implicit WENO Scheme ," *AIAA Journal*, vol. 47, pp. 331–344, 2009.

[32] J. Boling and G.-C. Zha, " Numerical Investigation of Co-Flow Jet 3D Transonic Wings." Proceedings of 2021 AIAA Aviation Virtual Forum, Aug. 2-6, 2021.